www.acsnano.org

# Comparing Multifunctional Viral and Eukaryotic Proteins for Generating Scission Necks in Membranes

Haleh Alimohamadi, Elizabeth Wei-Chia Luo, Shivam Gupta, Jaime de Anda, Rena Yang, Taraknath Mandal, and Gerard C. L. Wong\*



Downloaded via UNIV OF CALIFORNIA SANTA BARBARA on April 21, 2025 at 21:57:15 (UTC). See https://pubs.acs.org/sharingguidelines for options on how to legitimately share published articles.

Cite This: ACS Nano 2024, 18, 15545-15556



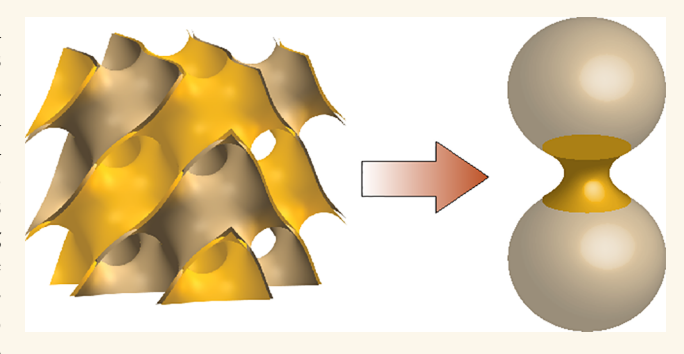
**ACCESS** 

III Metrics & More

Article Recommendations

Supporting Information

ABSTRACT: Deterministic formation of membrane scission necks by protein machinery with multiplexed functions is critical in biology. A microbial example is M2 viroporin, a proton pump from the influenza A virus that is multiplexed with membrane remodeling activity to induce budding and scission in the host membrane during viral maturation. In comparison, the dynamin family constitutes a class of eukaryotic proteins implicated in mitochondrial fission, as well as various budding and endocytosis pathways. In the case of Dnm1, the mitochondrial fission protein in yeast, the membrane remodeling activity is multiplexed with mechanoenzyme activity to create fission necks. It is not clear why these functions are



combined in these scission processes, which occur in drastically different compositions and solution conditions. In general, direct experimental access to changing neck sizes induced by individual proteins or peptide fragments is challenging due to the nanoscale dimensions and influence of thermal fluctuations. Here, we use a mechanical model to estimate the size of scission necks by leveraging small-angle X-ray scattering structural data of protein—lipid systems under different conditions. The influence of interfacial tension, lipid composition, and membrane budding morphology on the size of the induced scission necks is systematically investigated using our data and molecular dynamic simulations. We find that the M2 budding protein from the influenza A virus has robust pH-dependent membrane activity that induces nanoscopic necks within the range of spontaneous hemifission for a broad range of lipid compositions. In contrast, the sizes of scission necks generated by mitochondrial fission proteins strongly depend on lipid composition, which suggests a role for mechanical constriction.

KEYWORDS: lipid bilayer, scission necks, membrane-protein interactions, small-angle X-ray scattering, negative Gaussian curvature

Membrane neck formation is a critical step in many eukaryotic transport processes, such as endocytosis, exocytosis, and intracellular trafficking.<sup>1-3</sup> For microbial processes, vesicle budding and membrane neck formation also play crucial roles in the replication cycle of enveloped viruses and parasites.<sup>4-6</sup> In both classes of examples, the protein machinery often multiplexes membrane remodeling activity with drastically different functions. The formation of scission necks in eukaryotes is controlled by proteins that adsorb or insert into the cell membrane and reshape the membrane into distinct morphologies via different functions.<sup>7–9</sup> For example, dynamin-related GTPase proteins (Dnm1 in yeast, Drp1 in mammals) exhibit not only mechanoenzyme activity to "squeeze" fission necks but also the ability to remodel membrane curvature, thereby facilitating the formation of membrane necks in mitochondrial fission in a process that is not completely understood. <sup>10–14</sup> Similarly, bacterial pathogens

and viruses including rabies virus, parainfluenza virus-5, and influenza A possess protein machinery capable of membrane remodeling to enforce budding and scission in host cell membranes. However, this activity is also often combined with other functions. In the case of influenza A, the M2 viroporin that mediates budding is also a proton pump that can acidify local environments. Presently, these multiplexed functions are considered serendipitous accidents in evolution. There is no conceptual framework to see why these functions

Received: January 7, 2024 Revised: May 13, 2024 Accepted: May 22, 2024 Published: June 5, 2024





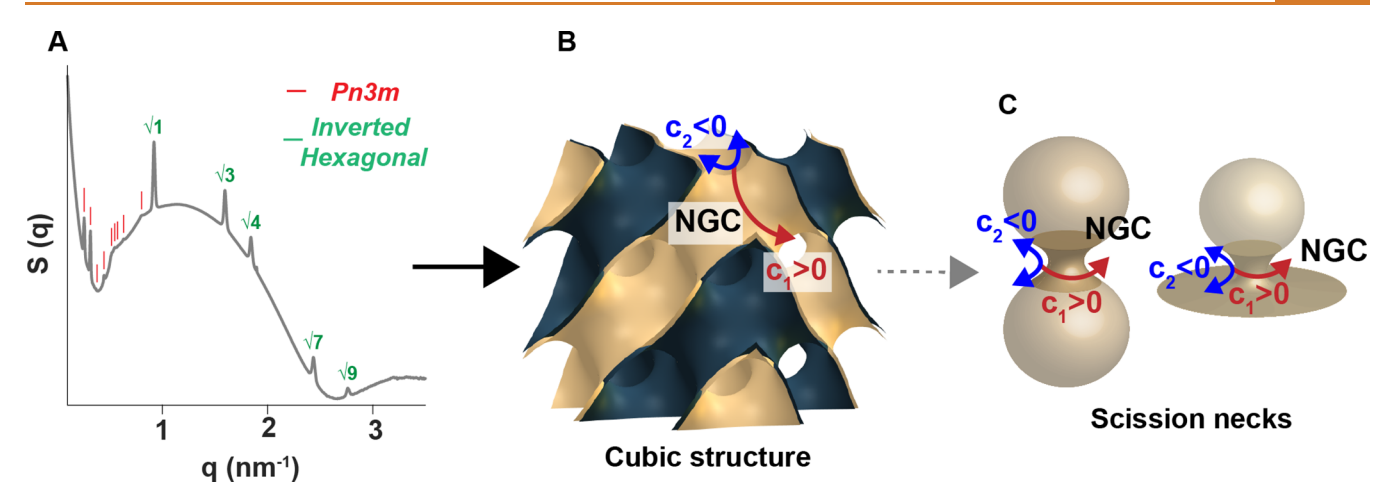


Figure 1. Estimating the induced radius of scission necks by membrane-remodeling proteins based on the membrane deformations observed in SAXS spectra. (A) SAXS spectra from a model mitochondrial membrane incubated with Dnm1, adapted with permission from ref 22. Copyright [2017] [American Chemical Society]. The peaks marked with red lines correspond to a Pn3m cubic phase with a lattice constant of 34.16 nm, and the set of correlation peaks with q-ratios of  $\sqrt{1}:\sqrt{3}:\sqrt{4}:\sqrt{7}:\sqrt{9}$  represents an inverted hexagonal structure with a lattice parameter of 7.88 nm. (B) 3D reconstruction of a Pn3m cubic phase with NGC ( $c_1 > 0$  and  $c_2$  cubic phase with NGC ( $c_1 > 0$  and  $c_2 < 0$ ) at every point. (C) Catenoid-shaped scission necks are characterized by NGC.

in particular are combined or whether the additional functions are somehow synergistic with membrane remodeling.

To understand the physicochemical principles underlying the membrane remodeling required for scission pores, it is important to experimentally determine the size and geometry of scission necks across a diverse range of experimental conditions, given that neck formation is distinct for different biological contexts (local lipid compositions) and local environmental conditions (pH, temperature). Various techniques including X-ray crystallography, 15 nuclear magnetic resonance spectroscopy (NMR), and electron microscopy (EM)<sup>17</sup> can in principle be used for estimating membrane curvatures in scission necks of reconstituted systems. However, these techniques are usually applicable only to specific experimental conditions that are amenable to the measurement itself (such as freezing or vacuum conditions). Moreover, measuring membrane neck sizes is further complicated by the dynamics of membrane deformations, the nanoscopic scale of neck formation, and the heterogeneous, transient, fluctuating nature of such structures. 18

Small-angle X-ray scattering (SAXS)<sup>19,20</sup> is a nondestructive technique that has been used to study the structure and phase behavior of biomolecular systems.<sup>21</sup> Specifically, using SAXS, previous studies have shown that pore-forming proteins can reorganize small unilamellar vesicles (SUVs) into bicontinuous cubic phases. 22-24 Cubic phases are periodic minimal surfaces that have been found in a wide range of membrane-bound organelles such as endoplasmic reticulum, Golgi apparatus, and mitochondrial membranes. <sup>25–28</sup> Cubic phases are idealized surfaces with zero mean curvature but rich in bilayer negative Gaussian curvature (NGC) (Figure 1). NGC is a geometric requirement of scission neck formation, so the observation of NGC-rich phases is consistent with the expectation (Figure 1). However, the precise quantitative relationship between the extent of induced curvatures observed in cubic phases (for instance, the NGC density per volume) and the actual dimensions of scission necks is not clear (Figure 1). The ability to estimate scission neck dimensions from the structure of cubic phases can have great utility since SAXS can be used for different lipid compositions and for different intensive

thermodynamic variables relevant to different biological environments.

The use of theoretical and computational methods integrated with experimental information has emerged as a potent approach for investigating induced membrane curvatures by proteins<sup>9,29-33</sup> and for distilling insights that are otherwise challenging to obtain. For example, Kozlovsky et al. have studied the role of proteins in membrane neck formation during fission and fusion processes. 30,34 They showed that for wide necks (neck radius > monolayer thickness), the necks adopt the shape of a catenoid with zero mean curvature.<sup>30</sup> Chabanon and Rangamani proposed that the Gaussian curvature of neck-like structures governs the distribution of the proteins in the neck region.<sup>31</sup> Dharmavaram et al. suggested that the mismatch between the Gaussian curvature of the partially assembled capsid as a spherical cap and the catenoid-shaped neck region creates an energy barrier during viral budding.<sup>2</sup>

In this study, we construct a minimal continuum elastic membrane model and use it to quantitatively extract protein-induced NGC from structures of cubic phases measured in SAXS. We apply the derived induced curvature as an input to the free energy of the membrane neck formation and estimate the radius of a stable scission neck via energy minimization. We introduce a dimensionless quantity, the "spontaneous scission number (SSN)", as a function of the cubic lattice constant, protein size, and size of the neck. The SSN controls the degree of the scission neck constriction, and we found that SSN > 1 is a threshold for the formation of necks sufficiently narrow to be within the range of possible spontaneous hemifission.

We apply our mechanical framework to estimate the size of scission necks induced by mitochondrial fission proteins in yeast (Dnm1) and the M2 budding protein from the influenza A virus, using measured cubic lattice constants. <sup>22,23</sup> We show that the degree of neck constriction by mitochondrial fission protein Dnm1 depends highly on lipid composition. Not only is this consistent with expectations for a highly regulated cellular process but it also suggests that the mechanoenzyme activity may be necessary to supplement the membrane

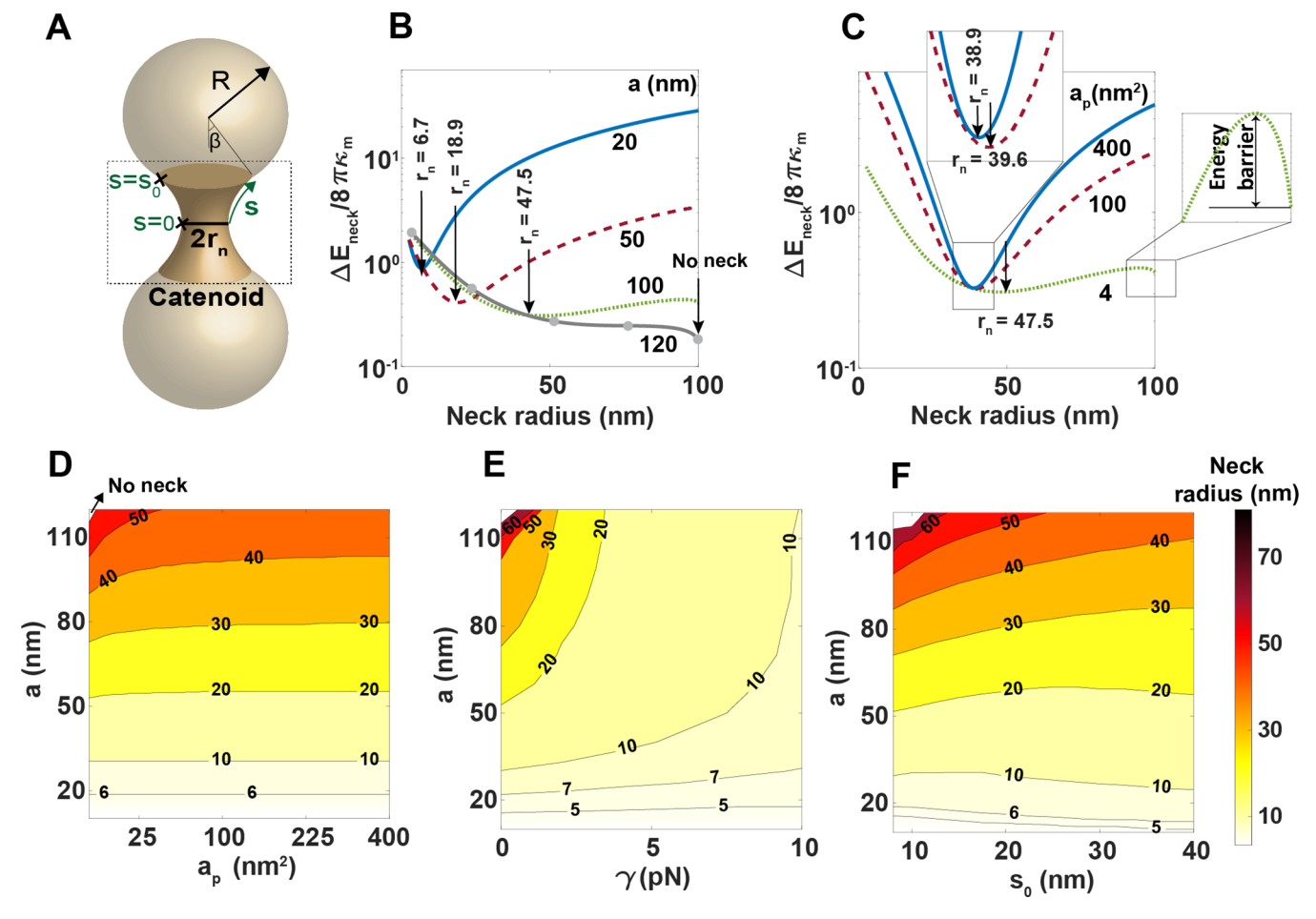


Figure 2. Estimating the radius of induced scission necks by membrane-remodeling proteins using the cubic structures in SAXS. (A) Idealized geometry of a membrane scission neck was modeled as a rotationally symmetric catenoid surface with a neck radius of  $r_n$  and two identical spherical caps with a radius of R. (B) Change in the energy of the system from a spherical vesicle to the idealized membrane scission neck geometry (eq 2) as the function of the neck radius for four different lattice constants ( $a_p = 4 \text{ nm}^2$ ,  $s_0 = 10 \text{ nm}$ , and  $\gamma = 0$ ). Arrows show the location of minimum energy corresponding to the stable radius of the constricted neck. The neck radius increases with the increasing lattice constant of cubic structures. (C) Change in the energy of the system as the function of the neck radius for three different protein surface areas in contact with the membrane at fixed a = 100 nm ( $s_0 = 10 \text{ nm}$  and  $\gamma = 0$ ). Larger proteins lead to a smaller scission neck, while at a small protein size, an energy barrier is associated with membrane neck constriction. Contour plot of the membrane scission neck radius for a range of (D) cubic lattice constants and protein surface area ( $s_0 = 10 \text{ nm}$  and  $\gamma = 0$ ), (E) cubic lattice constants and line tension ( $a_p = 4 \text{ nm}^2$  and  $s_0 = 10$ ), and (F) cubic lattice constants and catenoid length ( $s_0 = 4 \text{ nm}^2$  and  $s_0 = 10 \text{ nm}$ ). The white domains in panels (D), (E), and (F) mark the regions with no energy minima and no neck formation.

remodeling activity when lipid compositions are not optimal for membrane remodeling alone. In contrast, the M2 protein from influenza A infection is able to squeeze the budding neck to narrow sizes within the range of spontaneous hemifission in a manner that is significantly less sensitive to lipid composition. This is consistent with the need for the virus to successfully mature and bud in a broad range of eukaryotic cells with different lipid compositions. We demonstrate that a synthesized peptide of M2 protein, consisting of the transmembrane helix and the C-terminal cytoplasmic helix (M2TM-cyto), is sufficient to constrict vesicles and form narrow necks. Furthermore, we show that acidification in fact enhances the membrane remodeling activity of the M2 protein, which aligns with the activation of M2 channel proton transport upon acidification.<sup>35</sup> Using coarse-grained molecular dynamic simulations, we also illustrate that the M2 protein from influenza A virus can induce large anisotropic curvature independent of lipid composition. From these results, we

believe our framework can be generalized to other protein—membrane systems.

# **RESULTS AND DISCUSSION**

Estimation of the Radius of Induced Scission Necks by Membrane-Remodeling Proteins from SAXS Data. A range of proteins can remodel lipid membranes to form scission necks. The size of scission necks induced by proteins is a key geometric parameter in mediating different processes such as fission, fusion, and membrane trafficking. Here, we use our mechanical framework to estimate the radius of scission necks induced by membrane-remodeling proteins from SAXS measurements and systematically explore the influence of cubic lattice constant, protein area in contact with the membrane, and interfacial tension on the size of the scission necks.

We use the deviatoric curvature  $(D_0)$  estimated based on the lattice constants of cubic structures (here we used Pn3m) measured in SAXS as input to our model (Figure 2A). We plotted the change in the system (eq 2) from a spherical vesicle

to the idealized geometry of the scission neck as a function of the neck radius for four different cubic lattice constants in Figure 2B. Here, we set the effective surface area of the protein in contact with membrane  $(a_p) = 4 \text{ nm}^2$ ,  $s_0 = 10 \text{ nm}$ , and  $\gamma = 0$ . Considering an induced Pn3m cubic structure, we found that by decreasing the cubic lattice constants, e.g., a = 100 nm to a= 20 nm, the radius of the stable neck at the minimum energy reduces from  $r_n = 47.52$  nm to  $r_n = 6.75$  nm (arrows in Figure 2B). This implies that proteins that induce cubic phases with smaller lattice constants can strongly bend the membrane and significantly squeeze the scission neck (blue line in Figure 2B). The size of the scission neck increases almost as a quadratic function of the cubic lattice constant (Figure S2A). However, for large lattice constants (a > 110 nm), the change in the energy increases monotonically as the neck radius decreases (gray line in Figure 2B). This suggests that the induced deviatoric curvature by proteins is not strong enough to constrict the membrane and form the scission neck (gray line in Figure 2B).

The strength of interaction between the embedded proteins and the surrounding membrane depends on the surface area of proteins in contact with the membrane  $^{36,37}$  ( $a_{\rm p}$  in eq S10). Proteins with larger contact surface areas bind more strongly to the membrane and can constrict the membrane neck to smaller radii (Figure 2C, a=20 nm,  $s_0=10$  nm and  $\gamma=0$ ). In our model, the stronger membrane—protein interactions are equivalent to having a more negative Gaussian modulus at the protein domain (eq S10). Consistently, previous theoretical and experimental studies have shown that a more negative Gaussian modulus can facilitate membrane budding and the process of scission neck formation.  $^{38,39}$ 

In a free membrane without protein, scission neck formation is associated with an energy barrier due to the NGC of the neck and the negative Gaussian modulus of the membrane (eq S9).<sup>30,40</sup> This is analogous to the positive Gaussian energy barrier associated with transmembrane pore formation. Using our model to estimate the energy barrier associated with forming a simple catenoid-shaped neck (ignoring the spherical caps) from a spherical vesicle in a free membrane without protein, we observed that the height of the energy barrier increases with the magnitude of the Gaussian modulus and the vesicle size, and it decreases with an increase in the length of the catenoid (eq S9 and Figure S1). Interestingly, our results demonstrated that the interactions of curvaturegenerating proteins with the membrane decrease the height of the energy barrier and induce stable necks at a local energy minimum (Figure 2B,C). Based on our results, the energy barrier vanishes for (1) small cubic lattice constants corresponding to large induced deviatoric curvatures and (2) proteins with large contact surface area corresponding to stronger interactions with the membrane (Figure 2B,C). Similarly, we have previously shown that anisotropic curvature-generating peptides such as antimicrobial peptides decrease the energy barrier for transmembrane pore formation and stabilize pores in lipid bilayers.<sup>42</sup>

In biological contexts, membrane-remodeling proteins have a wide range of sizes and can alter their effective contact area with the membrane. We use our model to construct a contour plot of the induced scission neck for a range of cubic lattice constants and protein surface area in Figure 2D ( $s_0 = 10$  nm and  $\gamma = 0$ ). The vesicle remains undeformed, and there is no neck in a small domain with a very large cubic lattice constant and a small protein surface area (Figure 2D). Conversely,

narrow necks  $(r_n < 6 \text{ nm})$  can be formed for small cubic lattice constants (a < 16 nm), independent of the protein size (Figure 2D). We also found that for small cubic lattice constants, the size of the scission neck weakly depends on the interaction between the membrane and the proteins. Thus, to further squeeze the membrane neck and complete the scission phenomena, the induced line tension at the boundaries of protein phase separation can play an important role<sup>43</sup> (Figure 2E,  $a_p = 4 \text{ nm}^2$  and  $s_0 = 10 \text{ nm}$ ). For example, in the case of a =100 nm, increasing the magnitude of line tension from  $\gamma = 0$  to  $\gamma = 10 \text{ pN}^{44,45}$  results in an almost 80% decrease (from  $r_{\rm p} \sim$ 47.3 nm to  $r_{\rm n} \sim 9.7$  nm) in the radius of the scission neck (Figure 2E). Previous studies have also shown that an increase in the effective line tension, due to the insertion of the M2 transmembrane domain into the membrane, enhances curvature generation and vesicle budding. 46,47

Intuitively, one expects that the length of the catenoid  $(s_0)$  in the idealized geometry must affect the radius of the scission neck, as it defines the length scale of curvature modulation (Figure 2F,  $a_p = 4 \text{ nm}^2$  and  $\gamma = 0$ ). In our model, the length of the catenoid has a dual effect on the membrane-inclusion interaction energy (eq 1). On the one hand, an increase in the length of the catenoid leads to an increase in the area of the scission neck and the energy cost for membrane constriction. On the other hand, catenoids with larger lengths have smaller deviatoric curvatures  $(D = r_n/(r_n^2 + s_0^2))$ , which makes the formation of a narrow neck easier with a lower bending energy cost. The antagonistic effects of  $s_0$  on the elastic mismatch energy cost can be seen in Figure 2F. At small cubic lattice constants (a < 20 nm), the larger surface area of the catenoid becomes dominant in the elastic energy. Therefore, the neck radius increases with increasing the catenoid length (Figures 2F and S2B). However, at large lattice constants (a > 60 nm), the dominant term in the interaction energy is the membrane curvature. Thus, an increase in the catenoid length leads to a smaller neck radius (Figures 2F and S2C). Interestingly, at intermediate lattice constants (30 nm < a < 60 nm), we found that the neck radius is a nonmonotonic function of  $s_0$ ; as  $s_0$ increases, the neck radius decreases and then increases again (Figures 2F and S2D).

It is possible to construct a dimensionless quantity, the spontaneous scission number (SSN):

SSN =  $s_0\sqrt{a_{\rm p}}/a^2$  which combines the effects of the cubic lattice constant (a), protein surface area  $(a_{\rm p})$ , and catenoid length  $(s_0)$ . We found that SNN governs the formation of fission necks (Figure S3). As the SSN increases, the neck becomes smaller, and the radius of the neck is approximately proportional to the power function of the SSN,  $r_{\rm n} \sim {\rm SSN}^{-0.2}$  (Figure S3). Our findings suggested that SSN greater than 1 can give rise to the formation of sufficiently narrow necks (with radii below 5 nm) that allow spontaneous hemifission.

Morphology of Membrane Caps Influences the Radius of Induced Scission Necks by Membrane-Remodeling Proteins. Membrane budding is a common phenomenon that often takes place in large vesicles, known as "mother" vesicles, and results in the formation of smaller "daughter" vesicles. This process is observed in various cellular processes, such as clathrin-mediated endocytosis, the formation of synaptic vesicles, receptor-mediated endocytosis, and the viral replication cycle, where a small coated pit connects to a large mother vesicle via a neck-like structure. 5,48-53

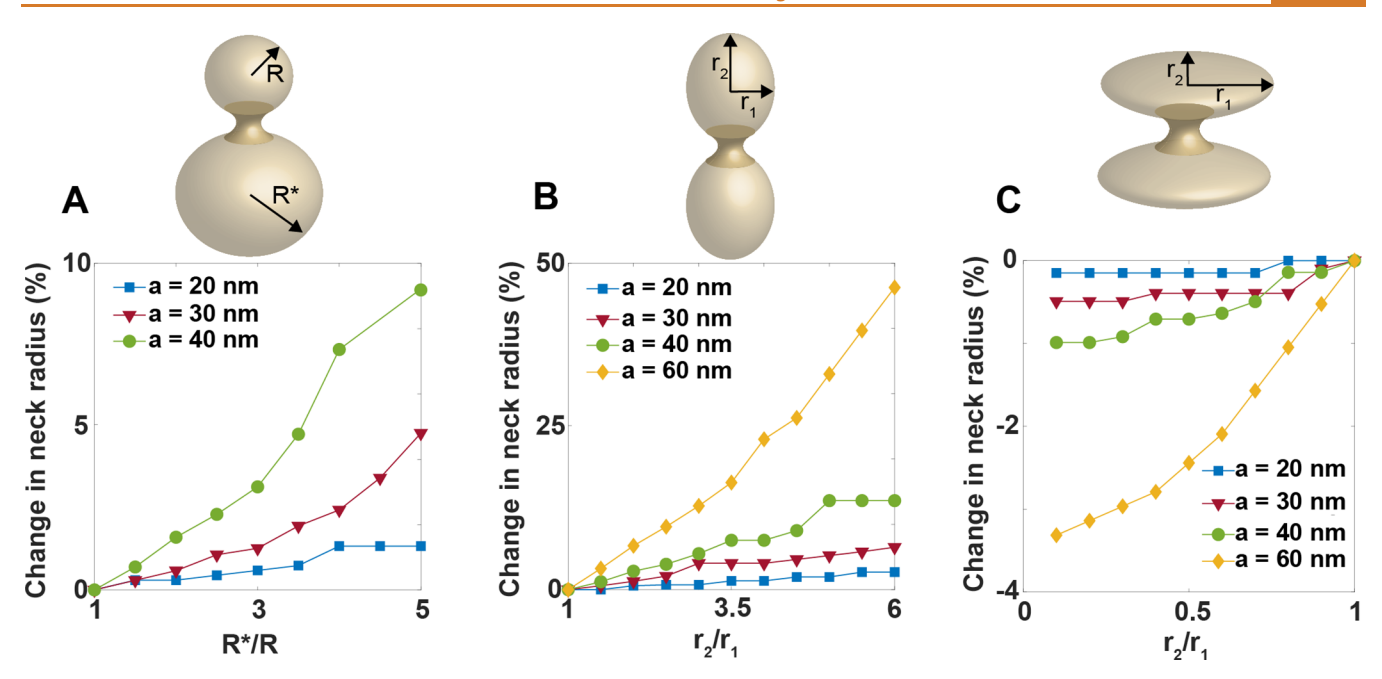


Figure 3. Effects of membrane cap morphology on the radius of induced scission neck by membrane-remodeling proteins. (A) Increase in the scission neck radius with increasing size ratio between two spherical caps  $(R^*/R)$ . The scission neck radius exhibits a more pronounced increase as a function of  $R^*/R$  for larger cubic lattice constants. (B) Increase in the scission neck radius with the increasing aspect ratio of the prolate-shaped caps. The size of the neck increases significantly ( $\sim$ 50%) when the aspect ratio increases from 1 (spherical caps) to 6 (prolate-shaped caps) at a=60 nm. (C) Decrease in the scission neck radius with decreasing aspect ratio of the oblate-shaped caps. For small cubic lattice constants (a<40 nm), the change in the neck radius is negligible (<1%). In all numerical calculations, we set  $a_p=4$  nm²,  $s_0=10$  nm, and  $\gamma=0$ .

To explore the robustness of neck formation by membraneremodeling proteins in large vesicles, we revised our idealized geometry and assumed that the spherical caps have two different radii, R and R\* (Figure 3A). Here, we set  $a_p = 4 \text{ nm}^2$ ,  $s_0 = 10$  nm, and  $\gamma = 0$  and plotted the percentage of change in neck radius compared to the case with two identical spherical caps,  $R^*/R = 1$  (Figure 3A). Based on our results, the scission neck gets wider with an increasing ratio of asymmetry between two spherical caps  $(R^*/R)$  (Figure 3A). The percentage of increase in the neck radius is proportional to the cubic lattice constant (Figure 3A). For example, for a = 20 nm, the neck radius increases less than 2% when  $R^*/R = 1$  increases to  $R^*/R$ = 5. However, our results show that for large lattice constants (a = 40 nm), there is a ~10% enlargement in the neck radius as the size of the mother vesicle increases to  $R^*/R = 5$  (Figure 3A).

We also investigated the impact of aspherical membrane cap morphology on the radius of induced scission necks by membrane-remodeling proteins (Figure 3B,C). This can be a representation of (I) the tubular membrane invagination in yeast endocytosis<sup>54</sup> and (II) the aspherical morphology of the membrane wrapping of elongated viruses such as coronavirus, Ebola, Marburg, and bullet-shaped Rhabdoviruses. <sup>55–59</sup> Influenza A virus is also known as a pleomorphic virus which displays a range of morphologies from filamentous to spherical. <sup>60</sup> Here, for simplicity, we only considered prolate-shaped caps with an aspect ratio  $(r_2/r_1) > 1$  (Figure 3B) and oblate-shaped caps with an aspect ratio <1 (Figure 3C).

We found that the size of the scission neck increases with an increase in the aspect ratio of the prolate-shaped cap (Figure 3B). Particularly, we observed that for large lattice constant (a = 60 nm), the radius of the scission neck increases  $\sim 50\%$  when increasing the aspect ratio from ratio = 1 to ratio = 6 (Figure

3B). For oblate-shaped caps, our results show that the neck radius slightly decreases (<4%) when decreasing the aspect ratio from ratio = 1 to ratio = 0.1 (Figure 3C). However, both prolate- and oblate-shaped caps create a large energy barrier in neck constriction (Figures S4 and S5). This could be related to the high membrane bending energy in ellipsoidal caps compared to the spherical caps. 61 We observed that the height of the energy barrier increases for larger lattice constants and is more dramatic in oblate-shaped caps (Figures S4 and S5). This is in agreement with previous theoretical and experimental studies, which have shown that the membrane engulfment time increases as the particle's shape deviates from a sphere. 62,63 Consistently, it has been suggested that the increase in internalization time is more dramatic for oblate shapes compared to prolate shapes. 62,63 Overall, these results suggest that the process of membrane budding from larger vesicles and with an aspherical cap morphology requires a higher degree of curvature induction by membrane-remodeling proteins.

Scission Neck from Viral Budding Protein Is Smaller than That from Mitochondrial Fission Proteins and Exhibits Different Lipid Requirements. It is interesting to test the model by comparing the behavior of induced scission necks by viral budding M2 protein from influenza A virus versus dynamin-mediated mitochondrial fission in eukaryotic cells. We have previously shown that Dnm1 and the M2 protein from influenza A virus can remodel lipid membranes to cubic structures with NGC.<sup>22,23</sup> Using these SAXS measurements as inputs for our model and estimating the effective surface area of proteins based on their X-ray crystallography, we calculated the radius of constricted necks induced by M2 protein and Dnm1 in different lipid compositions (Figure 4A). In these calculations, we considered 20% variations in the

protein surface area  $(a_p \pm 20\%)$  and the length of the neck  $(s_0 \pm 20\%)$ , assuming no line tension,  $\gamma = 0$  (Figure 4).

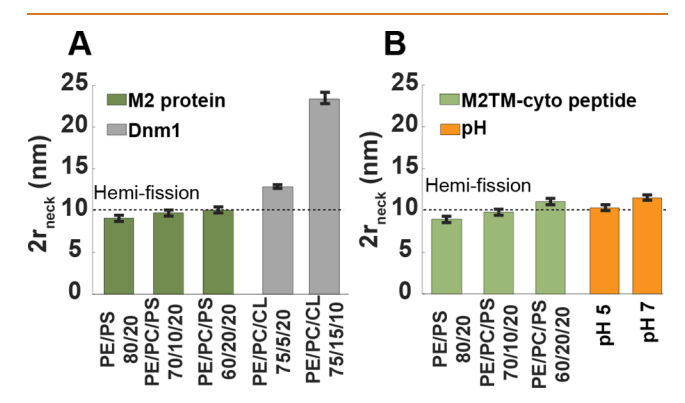


Figure 4. Comparison of membrane remodeling activity and induced scission necks by viral protein M2 from influenzas A and eukaryotic fission protein Dnm1. (A) Estimation of induced scission necks by M2 protein of influenza A virus and Dnm1 in different lipid compositions, using our mechanical framework and the cubic lattice constants measured in our previous SAXS experiments. <sup>22,23</sup> The M2 protein of influenza A virus can form narrow constricted necks <10 nm within the range of possible hemifission regime in different lipid compositions. (B) Estimation of induced scission necks by M2TM-cyto peptide in different lipid compositions, and the full-length M2 protein under neutral (pH 7) and acidic (pH 5) conditions. The M2 induces smaller scission neck sizes in acidic conditions. In both panels, we considered 20% variations in neck length ( $s_0 = 10$  nm) and effective contact surface area  $a_p$  ( $\gamma = 0$ ).

Based on our calculations, the size of induced fission necks by Dnm1 highly depends on the percentage of conical cardiolipin lipids present in the membrane (Figure 4A). For instance, in model membranes with ternary phospholipid mixtures of phosphatidylethanolamine (PE), phosphatidylcholine (PC), and cardiolipin (CL) at molar ratios of 75/5/20 and 75/15/10 PE/PC/CL, Dnm1 can constrict the membrane into catenoid-shaped necks with diameters ranging from 10.78 to 11.44 nm and 22.92-23.4 nm, respectively (Figure 4A). Previous studies have also shown that membrane lipid composition plays an important role in mitochondrial fission.<sup>64-66</sup> In particular, the presence of conical lipids in the mitochondrial membrane facilitates the interaction and activation of the GTPase domain of fission proteins. 64-66 Using a previously proposed catenoid-shaped neck model,<sup>30</sup> the average amount of Gaussian curvature in a cubic phase induced by Dnm1 in 75/5/20 PE/PC/CL model membrane maps to a fission neck of approximately 12.6 nm in diameter.<sup>22</sup> This is in agreement with our estimated neck size of 10.8 nm <  $2r_{\rm n}$  < 11.5 nm using the dumbbell-shaped constricted neck in our model (Figure 4A). In this context, it is interesting to note that connecting the catenoid-shaped neck to spherical caps with positive Gaussian curvature can decrease the size of the neck.

We employed our mechanical framework to estimate the size of the pinching neck generated by M2 proteins under different conditions; (I) the full length of M2 protein of the influenza A virus in different lipid membrane compositions<sup>23</sup> (Figure 4A), (II) a synthesized M2TM-cyto peptide in various lipid membrane compositions<sup>23</sup> (Figure 4B), (III) the full length of M2 protein in both neutral (pH 7) and acidic (pH 5) buffer conditions (Figure 4B). Here, we assume that the viral budding

occurs from a large vesicle, with a relative size ratio of  $R^*/R = 5$ . We found that both full-length M2 protein and the synthesized M2TM-cyto peptide can form narrow necks (neck diameter <10 nm) which can trigger the spontaneous membrane hemifission reaction<sup>67</sup> (Figure 4A,B). Interestingly, we found that, unlike fission proteins, the diameter of the endocytic neck generated by the M2 protein and the synthesized M2TM-cyto peptide does not strongly depend on the lipid composition (Figure 4A,B). This is interesting for several reasons. That viruses are much smaller than mitochondria places more stringent requirements for scission. Moreover, viruses, in principle, need to remodel host membranes with a wide range of lipid compositions.

The M2 viroporin is a proton pump as well as a membrane remodeling protein. We observed that under acidic conditions, the M2 protein from influenzas A induces tighter NGC and can constrict endocytic necks to narrow sizes that fall within the range of the spontaneous hemifission regime (Figure 4B). This indicates that the two functions of M2 both promote budding and do not act against one another. This could be attributed to a change in the backbone conformation of the C-terminal helices, which leads to altered lipid—protein interactions and induces anisotropic curvature, similar to the opening and activation of the influenza A M2 proton channel in response to acidification.<sup>35</sup>

M2 Protein from the Influenza A Virus Can Robustly Induce Anisotropic Curvature in a Range of Lipid Compositions in Coarse-Grained Molecular Dynamics **Simulations.** To test the predictions from the theoretical framework, we performed coarse-grained molecular dynamics simulation to compare the capability of the M2 protein of the influenza A virus versus Dnm1 to induce anisotropic curvature on flat membranes with two different lipid compositions (Figure 5). Previous studies have shown that the M2 proton channel and the pleckstrin homology (PH) domain of Dnm1 contain amphiphile loops that can insert into the lipid membrane and constrict the neck.<sup>23,68-71</sup> Using a previously trained support vector machine (SVM) classifier to assess the membrane-restructuring activity of a given protein sequence, we showed that both the M2 proton channel and the PH domain of Dnm1 contain amino acid sequences capable of remodeling membranes through anisotropic membrane curvature induction (Figure S6).

We placed a single transmembrane M2 proton channel at the center of a flat lipid bilayer with two different lipid compositions: (I) 80/20 PE/PS and (II) 75/15/10 PE/PC/ CL (Figure 5A,B). The system equilibrated for 2  $\mu$ s and we used the equilibrated trajectory to compute the deviatoric curvature generated on the membrane by the protein. The deviatoric curvature was calculated using the MDAnalysis tool and the VTK library of Python.<sup>73</sup> Details of the simulation protocol are described in the Supporting Information. We found that M2 protein can generate a similar degree of anisotropic curvature on both lipid compositions (Figure 5A,B). However, our results show that the induced anisotropic curvature in 75/15/10 PE/PC/CL lipid composition extends to a relatively larger distance compared to the 80/20 PE/PS flat lipid bilayer, which is likely due to the presence of flexible cardiolipins (Figure 5A,B). These simulation results are in agreement with predictions of our theoretical model and SAXS measurements that M2 protein can robustly induce deviatoric curvature on membranes with different lipid compositions.

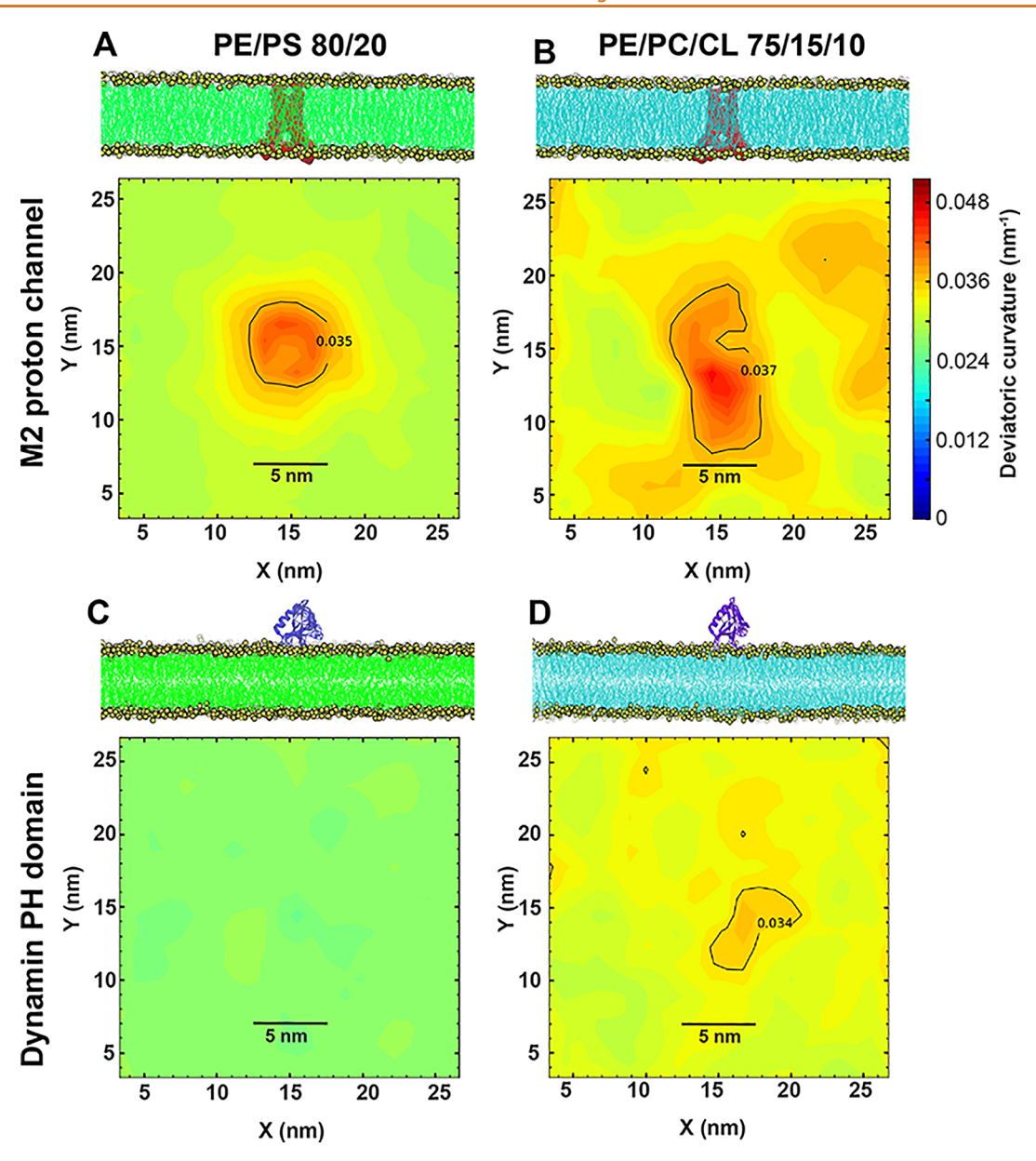


Figure 5. M2 protein from the influenza A virus induces robust anisotropic curvature independent of the membrane lipid composition in molecular dynamics simulations. Structure of the protein—membrane complex (upper panel) and contour plot of the deviatoric curvature generated by the protein on the membrane surface (lower panel) for (A) M2 proton channel from the influenza A virus on PE/PS 80/20 lipid bilayer, (B) M2 proton channel from the influenza A virus on PE/PC/CL 75/15/10 lipid bilayer, (C) dynamin PH domain on 80/20 PE/PS lipid bilayer, and (D) dynamin PH domain on PE/PC/CL 75/15/10 lipid bilayer. M2 protein and dynamin PH domain are shown by the red and violet colors, respectively.

As expected, deviatoric curvature generated by the PH domain of Dnm1 strongly depends on the lipid composition of the membrane. While it induces a decent amount of deviatoric curvature on the 75/15/10 PE/PC/CL membrane, it does not generate any deviatoric curvature near the location of the protein on the 80/20 PE/PS membrane (Figure 5C,D). We also observed that the magnitude of the induced deviatoric curvature by the M2 protein is higher than the PH domain on both lipid compositions (Figure 5). The curvature generated by the M2 protein also extends to a relatively larger distance compared to the induced curvature by the PH domain. Additionally, we plotted the radius of curvature of the membrane deformations  $(1/\sqrt{|c_1c_2|})$  induced by the Dnm1 and M2 protein from influenza A in two different lipid

compositions (Figure S7). As expected, the larger magnitude of curvature induced by M2 protein, compared to Dnm1, results in more significant membrane remodeling and a smaller radius of curvature, which does not depend on the lipid composition (Figure S7). These results suggest that neck formation by the dynamin-related family of proteins strongly depends on the lipid composition, while the M2 protein from the influenza A virus can form narrow scission necks over a range of cell membranes with different lipid compositions.

### **CONCLUSIONS**

In summary, we present a minimal mechanical model to directly use SAXS measurements to estimate the radius of scission necks induced by membrane-remodeling proteins. Using this method, it is possible to systematically explore the interplay between the protein surface area, the magnitude of induced curvatures by proteins, interfacial tension at the phaseseparated protein boundary, and the morphology of the caps in regulating the size of scission necks (Figures 2 and 3). In particular, we introduce a dimensionless quantity, the "spontaneous scission number = (catenoid length)(  $\sqrt{\text{protein surface area}}$  /(cubic lattice constant)<sup>2</sup>" which characterizes the extent of scission neck constriction (Figure 2). Our results also show that the neck radius depends on the morphology and symmetry of caps (Figure 3). For instance, for large lattice constants, the neck radius increases noticeably for membrane budding from a large vesicle ( $\sim$ 10%) and with prolate-shaped caps (~50%) (Figure 3). Additionally, we find that for ellipsoidal-shaped caps, neck constriction is associated with a large energy barrier ( $\sim$ 1500kT) (Figures S4 and S5). This substantial energy barrier implies that a secondary mechanism such as actin-mediated pinching forces or helical twist is required to complete fission. 54,74,7

In the general context of required NGC for membrane remodeling in scission necks versus transmembrane pore formation, we observe that the energy barrier associated with the formation of transmembrane pores 42,76 is almost 6x larger compared to the energy barrier involved in the neck constriction process (identical spherical caps in Figure 2). Additionally, we identify that scission necks can be formed across a wide range of cubic lattice constants, 0 < a < 100 nm (Figure 2), whereas pore formation is confined to a relatively narrow range of lattice constants (0 < a < 30 nm). <sup>42</sup> Thus, we predict that the membrane remodeling required for scission neck formation is simpler than the initiation of transmembrane pore opening. We find that the proton pumping activity of M2 viroporin does not interfere with its membrane remodeling activity. In fact, the two activities appear to be synergistic. It would be interesting to investigate other pH-dependent microbial pore-formers, such as diphtheria toxin. method presented here is potentially applicable to other protein-induced membrane-remodeling processes such as budding, blebbing, and tubulation and can provide insight into the mechanical design principles for robust vesiculation, e.g., in drug or gene delivery systems.

Despite the agreement of our model predictions with experimental data, we acknowledge some limitations and simplifying assumptions of our model. We used an idealized geometry of scission neck, including a rotationally symmetric catenoid surface with zero mean curvature connected to spherical caps. However, the geometry of a scission neck is more complicated: the neck is not a complete catenoid, and the caps can have arbitrary shapes. Thus, future efforts will focus on including the 3D asymmetric morphology of scission neck formation.<sup>78</sup> Additionally, we assumed that the NGCgenerating inclusions are confined to the neck region and that the outer surface area of the neck is fully covered by NGCgenerating proteins (protein saturation). However, two aspects can be incorporated into future studies: (I) the dependency of the deviatoric curvature and neck constriction on protein concentration and (II) the contribution of entropic term due to the heterogeneous distribution of proteins on the membrane surface. 79,80 In the current model, we focused only on the role of induced anisotropic curvature by membrane remodeling proteins in regulating scission neck formation. However, membrane budding, e.g., viral budding, is governed by a complex interactive machinery of proteins, ligands, and

receptors.<sup>81–84</sup> Thus, for a more general model, these effects should be considered. Finally, we studied the pH-dependent membrane activity of the M2 protein from influenza A in one lipid composition at two different pH levels (Figure 4). Future efforts focusing on other pH-dependent membrane remodeling proteins across various lipid compositions and environments will be important for identifying the quantitative relationship between pH level and the degree of induced curvature.

## **METHODS**

**Membrane Mechanics.** We model the lipid bilayer as a thin elastic shell with negligible thickness compared to the radii of membrane curvature. S5,86 We assume the membrane is incompressible since the energetic cost of stretching the membrane is much higher than membrane bending. We also assume that NGC-generating inclusions are confined in the neck region based on previous studies that have shown fission and viral proteins, such as Dnm1 and M2 protein from influenza A, can sense the membrane curvature and entropic forces localize them at the scission necks in order to facilitate the constriction process. Furthermore, we assume that membrane inclusions are more rigid than the lipid bilayer and use the augmented version of the Helfrich—Canham energy to model the membrane—protein interactions. Assuming the system is at mechanical equilibrium at all times, the total energy of the system (E) is given by 43,90—94

$$E = \int_{A_{\text{protein}}} \left(2K_{\text{l,p}} + K_{\text{2,p}}\right) (H - H_0)^2 - K_{\text{2,p}} (D - D_0)^2 dA$$

$$\frac{\text{membrane-protein interaction energy}}{\text{membrane}} + \int_{A_{\text{free-membrane}}} 2\kappa_{\text{m}} H^2 + \kappa_{\text{G,m}} K dA + \gamma \oint dl$$

$$\frac{1}{\text{membrane-bending energy}} \text{line tensionenergy}$$
 (1)

where the first term corresponds to the mismatch elastic energy between the local shape of the lipid membrane and the intrinsic shape of the inclusion in the neck region and the second term indicates the membrane bending energy in the domain with no inclusion. The third term in eq 1 represents the energy cost due to the phase separation of NGC-generating inclusions at the scission necks, and the discontinuity in the idealized morphology of the scission neck, where the catenoid-shaped neck with zero mean curvature connects to the spherical cap with positive mean curvature (analogous to the cup-like model).  $^{43,45,95,96}$  In eq 1,  $K_{1,p}$  and  $K_{2,p}$  are constants ( $K_{1,p} > 0$  and  $K_{2,p}$ < 0) representing the strength of interaction between the inclusions and the surrounding membrane.  $^{93,94}$   $\kappa_{\rm m}$  and  $\kappa_{\rm G,m}$  are the bending and Gaussian moduli of the lipid bilayer, respectively. H is the mean curvature, D is the curvature deviator, and K is the Gaussian curvature of the lipid membrane  $(D^2 = H^2 - K)$ .  $H_0$  is the spontaneous mean curvature,  $D_0$  is the intrinsic deviatoric curvature, and  $\gamma$  is line tension at the neck boundary. The augmented version of Helfrich energy in eq 1 allows us to account for the effect of induced anisotropic curvature by scission proteins, which is energetically required for remodeling the lipid membrane into cylindrical and neck-shaped structures.

With no induced curvatures ( $H_0=0$  and  $D_0=0$ ), the membrane—protein interaction energy in eq 1 reduces to the classical Helfrich energy with quadratic dependence on mean curvature and linear dependence on Gaussian curvature,  $W_{\rm membrane-protein\ interaction}=2K_{1,p}H^2+K_{2,p}K$ , where  $K_{1,p}$  represents the bending rigidity and  $K_{2,p}$  indicates the Gaussian modulus of the membrane covered by curvature-generating proteins. It should be mentioned that in eq 1, we assume that the contribution of entropic energy is small compared to the membrane—protein interactions energy,  $\frac{K_{1,p-2,p}}{kT}\gg 1$ , where k is the Boltzmann constant, and T is temperature. Additionally, we assume the outer surface area of the neck is fully covered by NGC-generating proteins, and the first integral is taken over the area of the membrane that is covered by NGC-generating inclusions ( $A_{\rm protein-covered}$ ), while

the second integral is taken over the bare lipid bilayer with no inclusion ( $A_{\rm free-membrane}$ ).

Free Energy of Scission Neck Formation. To establish a relationship between the induced curvatures by membrane-remodeling proteins such as Drp1 observed in SAXS to the actual size of scission necks, we assume that proteins remodel a spherical vesicle with a radius of  $R_{\rm s}=100$  nm (approximate size of a SUV in SAXS) to an idealized geometry of mitochondrial fission. The idealized geometry of membrane fission includes a rotationally symmetric catenoid surface with a neck radius of  $r_{\rm n}$  and two spherical caps with a radius of R (Figure 2A). This simplified geometry has been widely used in previous studies to model local neck structures, viral budding, and membrane fission.  $^{29-32}$  The excess free energy of the system (including membrane and proteins) with respect to the vesicle can be written as (details in eq S7)

$$\Delta E_{\text{neck}} = -\frac{2\pi K_{2,p}}{\sqrt{r_n^2 + s_0^2}} \left[ s_0 (r_n^2 D_0^2 + D_0^2 s_0^2 + 2) + r_n^2 D_0 (r_n D_0 - 4) \sqrt{\frac{s_0^2}{r_n^2} + 1} \sinh^{-1} \left( \frac{s_0}{r_n} \right) \right]$$

$$+ 2\pi \left( 2K_{1,p} + K_{2,p} \right) H_0^2 \left[ s_0 \sqrt{r_n^2 + s_0^2} + r_n^2 \log \left( \sqrt{r_n^2 + s_0^2} + s_0 \right) - r_n^2 \log(r_n) \right] + 8\pi \kappa_m \left( 1 - \frac{\beta}{\pi} \right)$$

$$+ 4\pi \gamma \sqrt{r_n^2 + s_0^2} - 4\pi \kappa_m$$

$$(2)$$

where  $\kappa_{\rm m}$  is the membrane bending rigidity,  $\beta$  is the angle between the vertical axis and edge of the disk forming at the base of the catenoid, and  $s_0$  is the length of the catenoid (Figure 2A). For simplicity, in eq 2, we set  $\kappa_{\rm G,m}$  (membrane Gaussian modulus)  $\sim -\kappa_{\rm m}$ . 101

The magnitude of induced deviatoric curvature can be estimated from the cubic structure formed by membrane-remodeling proteins in SAXS, given as 42

$$D_0|_{\text{energy minimazation}} = \langle D \rangle = \sqrt{\frac{2\pi\chi}{A^*a^2}}$$
 (3)

where a is the lattice parameter,  $\chi$  is the Euler characteristic, and  $A^*$  is the dimensionless surface area per unit cell specific to each cubic phase. 102,103 Using the structure of cubic phases and inverted hexagonal structures formed by the scission neck protein machinery, such as dynamin and the M2 protein from influenza A, in SAXS measurements,  $^{22,23}$  we estimated that  $D_0$  (estimated based on eq 3) is almost 3–4 times larger than  $H_0$   $(H_0 \sim \frac{1}{2H_{\rm II}})$ , where  $H_{\rm II}$  is the lattice constant of the inverted hexagonal phase). Thus, for simplicity, we ignored the contribution of  $H_0$  in the rest of our calculation. Assuming the total area of the membrane remains constant ( $A_{\text{sphere vesicle}}$  = Aidealized-neck-geometry), for each given radius of the neck (fixed catenoid length), we first numerically calculated the angle  $\beta$ . Then, we numerically calculate the excess energy of neck formation at the given neck radius (eq 2) and the amount of induced deviatoric curvature from SAXS data (eq 3) to find the neck radius  $(r_n)$  that minimizes  $\Delta E_{\rm neck}$ . In our calculations, we estimated the strength of interaction between the membrane and protein  $(K_{2,p})$  based on the elastic properties of the membrane and the size of the inclusions (eq S10). The details of the derivations and complete equations are provided in the Supporting Information.

## **ASSOCIATED CONTENT**

# Supporting Information

The Supporting Information is available free of charge at https://pubs.acs.org/doi/10.1021/acsnano.4c00277.

This manuscript is a version of a preprint that was originally submitted and available online (accessed 07-

01-2024). H. Alimohamadi, E. W. C Luo, S. Gupta, J.D. Anda, R. Yang, T. Mandal, and G. C. L. Wong. Comparing multifunctional viral and eukaryotic proteins for generating scission necks in membranes. 2024. 574447. bioRxiv, 10.1101/2024.01.05.574447. Energy barrier in neck constriction as a function of vesicle size, neck length, and Gaussian modulus; scission neck size as a function of cubic lattice constant and catenoid length; variation of a neck radius as a function of the spontaneous scission number; change in the energy of the system from a spherical vesicle to the idealized scission neck geometry with prolate- and oblate-shaped caps; heatmaps of  $\sigma$  scores from an SVM classifier for the M2 proton channel and Dnm1 PH domain; and contour plot of induced radius of curvature by the M2 proton channel and Dnm1 PH domain (PDF)

## **AUTHOR INFORMATION**

# **Corresponding Author**

Gerard C. L. Wong — Department of Bioengineering, University of California, Los Angeles, Los Angeles, California 90025, United States; Department of Chemistry and Biochemistry, University of California, Los Angeles, California 90095, United States; Department of Microbiology, Immunology, and Molecular Genetics and California NanoSystems Institute, University of California, Los Angeles, California 90095, United States; orcid.org/0000-0003-0893-6383; Email: gclwong@seas.ucla.edu

#### **Authors**

Haleh Alimohamadi — Department of Bioengineering,
University of California, Los Angeles, Los Angeles, California
90025, United States; Department of Chemistry and
Biochemistry, University of California, Los Angeles,
California 90095, United States; Department of
Microbiology, Immunology, and Molecular Genetics and
California NanoSystems Institute, University of California,
Los Angeles, California 90095, United States; orcid.org/
0000-0001-6576-2426

Elizabeth Wei-Chia Luo — Department of Bioengineering, University of California, Los Angeles, Los Angeles, California 90025, United States; Department of Chemistry and Biochemistry, University of California, Los Angeles, California 90095, United States; Department of Microbiology, Immunology, and Molecular Genetics and California NanoSystems Institute, University of California, Los Angeles, California 90095, United States; orcid.org/0000-0002-8663-0446

Shivam Gupta — Department of Physics, Indian Institute of Technology Kanpur, Kanpur 208016, India

Jaime de Anda — Department of Bioengineering, University of California, Los Angeles, Los Angeles, California 90025, United States; Department of Chemistry and Biochemistry, University of California, Los Angeles, California 90095, United States; Department of Microbiology, Immunology, and Molecular Genetics and California NanoSystems Institute, University of California, Los Angeles, California 90095, United States; orcid.org/0000-0003-2129-0775

Rena Yang — Department of Bioengineering, University of California, Los Angeles, Los Angeles, California 90025, United States; Department of Chemistry and Biochemistry, University of California, Los Angeles, California 90095, United States; Department of Microbiology, Immunology, and Molecular Genetics and California NanoSystems Institute, University of California, Los Angeles, California 90095, United States

Taraknath Mandal — Department of Physics, Indian Institute of Technology Kanpur, Kanpur 208016, India

Complete contact information is available at: https://pubs.acs.org/10.1021/acsnano.4c00277

#### **Author Contributions**

H.A. designed the research and G.C.L.W. supervised the research. T.M. and S.G. conducted the molecular dynamics simulations. H.A, E.W.C.L., J.D.A., R.Y., and G.C.L.W. wrote the manuscript. All authors reviewed and approved the final version of the manuscript.

#### Notes

The authors declare no competing financial interest.

# **ACKNOWLEDGMENTS**

This work was supported by the American Heart Association (AHA 966662) grant to G.C.L.W. and by the BioPACIFIC Materials Innovation Platform of the National Science Foundation under Award No. DMR-1933487. H.A. was supported by the Vascular Biology Training Grant (T32 HL069766-21). J.D.A. was supported by the NSF Graduate Research Fellowship Program (DGE-1650604). T.M. gratefully acknowledges the support from the Government of India: Science and Engineering Research Board via Sanction No. SRG/2022/000548. We thank the Stanford Synchrotron Radiation Lightsource (SSRL) (Menlo Park, CA, USA) for access to beamline 4-2. Use of the SSRL, SLAC National Accelerator Laboratory, is supported by the U.S. Department of Energy, Office of Science, Office of Basic Energy Sciences under contract no. DE-AC02-76SF00515. The SSRL Structural Molecular Biology Program is supported by the U.S. Department of Energy, Office of Biological and Environmental Research, and by the National Institutes of Health, National Institute of General Medical Sciences (including P30GM133894). T.M. is grateful for the computational resources provided by PARAM Sanganak under the National Supercomputing Mission, Government of India, at the Indian Institute of Technology, Kanpur.

# **REFERENCES**

- (1) Hurley, J. H.; Hanson, P. I. Membrane Budding and Scission by the ESCRT Machinery: It's All in the Neck. *Nat. Rev. Mol. Cell Biol.* **2010**, *11* (8), 556–566.
- (2) Kukulski, W.; Schorb, M.; Kaksonen, M.; Briggs, J. A. G. Plasma Membrane Reshaping during Endocytosis Is Revealed by Time-Resolved Electron Tomography. *Cell* **2012**, *150* (3), 508–520.
- (3) Ren, G.; Vajjhala, P.; Lee, J. S.; Winsor, B.; Munn, A. L. The BAR Domain Proteins: Molding Membranes in Fission, Fusion, and Phagy. *Microbiology and Molecular Biology Reviews* **2006**, 70 (1), 37–120.
- (4) Chen, B. J.; Lamb, R. A. Mechanisms for Enveloped Virus Budding: Can Some Viruses Do without an ESCRT? *Virology* **2008**, 372 (2), 221–232.
- (5) Pornillos, O.; Garrus, J. E.; Sundquist, W. I. Mechanisms of Enveloped RNA Virus Budding. *Trends Cell Biol.* **2002**, *12* (12), 569–579.
- (6) Rossman, J. S.; Jing, X.; Leser, G. P.; Lamb, R. A. Influenza Virus M2 Protein Mediates ESCRT-Independent Membrane Scission. *Cell* **2010**, *142* (6), 902–913.

- (7) McMahon, H. T.; Gallop, J. L. Membrane Curvature and Mechanisms of Dynamic Cell Membrane Remodelling. *Nature* **2005**, 438 (7068), 590–596.
- (8) Zimmerberg, J.; Kozlov, M. M. How Proteins Produce Cellular Membrane Curvature. *Nat. Rev. Mol. Cell Biol.* **2006**, *7* (1), 9–19.
- (9) Alimohamadi, H.; Rangamani, P. Modeling Membrane Curvature Generation Due to Membrane-Protein Interactions. *Biomolecules* **2018**, *8* (4), 120.
- (10) Antonny, B.; Burd, C.; De Camilli, P.; Chen, E.; Daumke, O.; Faelber, K.; Ford, M.; Frolov, V. A.; Frost, A.; Hinshaw, J. E.; Kirchhausen, T.; Kozlov, M. M.; Lenz, M.; Low, H. H.; McMahon, H.; Merrifield, C.; Pollard, T. D.; Robinson, P. J.; Roux, A.; Schmid, S. Membrane Fission by Dynamin: What We Know and What We Need to Know. *EMBO J.* **2016**, 35 (21), 2270–2284.
- (11) Otsuga, D.; Keegan, B. R.; Brisch, E.; Thatcher, J. W.; Hermann, G. J.; Bleazard, W.; Shaw, J. M. The Dynamin-Related GTPase, Dnm1p, Controls Mitochondrial Morphology in Yeast. *J. Cell Biol.* **1998**, *143* (2), 333–349.
- (12) Bleazard, W.; McCaffery, J. M.; King, E. J.; Bale, S.; Mozdy, A.; Tieu, Q.; Nunnari, J.; Shaw, J. M. The Dynamin-Related GTPase Dnm1 Regulates Mitochondrial Fission in Yeast. *Nat. Cell Biol.* **1999**, 1 (5), 298–304.
- (13) Smirnova, E.; Griparic, L.; Shurland, D. L.; van der Bliek, A. M. Dynamin-Related Protein Drp1 Is Required for Mitochondrial Division in Mammalian Cells. *Mol. Biol. Cell* **2001**, *12* (8), 2245–2256.
- (14) Smirnova, E.; Shurland, D. L.; Ryazantsev, S. N.; van der Bliek, A. M. A Human Dynamin-Related Protein Controls the Distribution of Mitochondria. *J. Cell Biol.* **1998**, *143* (2), 351–358.
- (15) Shi, Y. A Glimpse of Structural Biology through X-Ray Crystallography. Cell 2014, 159 (5), 995–1014.
- (16) Marion, D. An Introduction to Biological NMR Spectroscopy \*. Molecular & Cellular Proteomics 2013, 12 (11), 3006–3025.
- (17) Beckett, A. J.; Prior, I. A. Electron Microscopy Methods for Studying Plasma Membranes. *Methods Mol. Biol.* **2015**, *1232*, 137–151.
- (18) Groves, J. T.; Parthasarathy, R.; Forstner, M. B. Fluorescence Imaging of Membrane Dynamics. *Annu. Rev. Biomed Eng.* **2008**, *10*, 311–338.
- (19) Brogden, K. A. Antimicrobial Peptides: Pore Formers or Metabolic Inhibitors in Bacteria? *Nat. Rev. Microbiol* **2005**, 3 (3), 238–250.
- (20) Epand, R. M.; Vogel, H. J. Diversity of Antimicrobial Peptides and Their Mechanisms of Action. *Biochimica et Biophysica Acta (BBA)* -. *Biomembranes* 1999, 1462 (1), 11–28.
- (21) Svergun, D. I.; Koch, M. H. J. Small-Angle Scattering Studies of Biological Macromolecules in Solution. *Rep. Prog. Phys.* **2003**, *66* (10), 1735.
- (22) Lee, M. W.; Lee, E. Y.; Lai, G. H.; Kennedy, N. W.; Posey, A. E.; Xian, W.; Ferguson, A. L.; Hill, R. B.; Wong, G. C. L. Molecular Motor Dnm1 Synergistically Induces Membrane Curvature To Facilitate Mitochondrial Fission. *ACS Cent. Sci.* **2017**, 3 (11), 1156–1167.
- (23) Schmidt, N. W.; Mishra, A.; Wang, J.; DeGrado, W. F.; Wong, G. C. L. Influenza Virus A M2 Protein Generates Negative Gaussian Membrane Curvature Necessary for Budding and Scission; ACS Publications. DOI: 10.1021/ja4001462.
- (24) Lee, M. W.; Luo, E. W.-C.; Silvestre-Roig, C.; Srinivasan, Y.; Akabori, K.; Lemnitzer, P.; Schmidt, N. W.; Lai, G. H.; Santangelo, C. D.; Soehnlein, O. Apolipoprotein Mimetic Peptide Inhibits Neutrophil-Driven Inflammatory Damage via Membrane Remodeling and Suppression of Cell Lysis. ACS Nano 2021, 15 (10), 15930–15939.
- (25) Deng, Y.; Mieczkowski, M. Three-Dimensional Periodic Cubic Membrane Structure in the Mitochondria of Amoebae Chaos Carolinensis. *Protoplasma* **1998**, 203 (1), 16–25.
- (26) Snapp, E. L.; Hegde, R. S.; Francolini, M.; Lombardo, F.; Colombo, S.; Pedrazzini, E.; Borgese, N.; Lippincott-Schwartz, J.

- Formation of Stacked ER Cisternae by Low Affinity Protein Interactions. J. Cell Biol. 2003, 163 (2), 257–269.
- (27) Almsherqi, Z. A.; Kohlwein, S. D.; Deng, Y. Cubic Membranes: A Legend beyond the Flatland\* of Cell Membrane Organization. *J. Cell Biol.* **2006**, *173* (6), 839–844.
- (28) Chabanon, M.; Rangamani, P. Geometric Coupling of Helicoidal Ramps and Curvature-Inducing Proteins in Organelle Membranes. *Journal of The Royal Society Interface* **2019**, *16* (158), No. 20190354.
- (29) Dharmavaram, S.; She, S. B.; Lázaro, G.; Hagan, M. F.; Bruinsma, R. Gaussian Curvature and the Budding Kinetics of Enveloped Viruses. *PLoS Comput. Biol.* **2019**, *15* (8), No. e1006602.
- (30) Kozlovsky, Y.; Kozlov, M. M. Membrane Fission: Model for Intermediate Structures. *Biophys. J.* **2003**, *85* (1), 85–96.
- (31) Chabanon, M.; Rangamani, P. Gaussian Curvature Directs the Distribution of Spontaneous Curvature on Bilayer Membrane Necks. *Soft Matter* **2018**, *14* (12), 2281–2294.
- (32) Kurioz, P.; Mesarec, L.; Iglič, A.; Kralj, S. Assembling of Topological Defects at Neck-Shaped Membrane Parts. *physica status solidi* (a) **2019**, 216 (13), No. 1800722.
- (33) Alimohamadi, H.; Vasan, R.; Hassinger, J.; Stachowiak, J.; Rangamani, P. The Role of Traction in Membrane Curvature Generation. *Biophys. J.* **2018**, *114* (3), 600a.
- (34) Chernomordik, L. V.; Kozlov, M. M. Protein-Lipid Interplay in Fusion and Fission of Biological Membranes. *Annu. Rev. Biochem.* **2003**, 72, 175–207.
- (35) Liang, R.; Swanson, J. M. J.; Madsen, J. J.; Hong, M.; DeGrado, W. F.; Voth, G. A. Acid Activation Mechanism of the Influenza A M2 Proton Channel. *Proc. Natl. Acad. Sci. U. S. A.* **2016**, *113* (45), E6955–E6964.
- (36) Fošnarič, M.; Kralj-Iglič, V.; Bohinc, K.; Iglič, A.; May, S. Stabilization of Pores in Lipid Bilayers by Anisotropic Inclusions. *J. Phys. Chem. B* **2003**, *107* (45), 12519–12526.
- (37) May, S. Membrane Perturbations Induced by Integral Proteins: Role of Conformational Restrictions of the Lipid Chains. *Langmuir* **2002**, *18* (16), 6356–6364.
- (38) Jülicher, F.; Lipowsky, R. Shape Transformations of Vesicles with Intramembrane Domains. *Phys. Rev. E* **1996**, *53* (3), 2670–2683.
- (39) Baumgart, T.; Das, S.; Webb, W. W.; Jenkins, J. T. Membrane Elasticity in Giant Vesicles with Fluid Phase Coexistence. *Biophys. J.* **2005**, 89 (2), 1067–1080.
- (40) Siegel, D. P. The Gaussian Curvature Elastic Energy of Intermediates in Membrane Fusion. *Biophys. J.* **2008**, 95 (11), 5200–5215
- (41) Schmidt, N. W.; Wong, G. C. Antimicrobial Peptides and Induced Membrane Curvature: Geometry, Coordination Chemistry, and Molecular Engineering. *Curr. Opin. Solid State Mater. Sci.* **2013**, 17 (4), 151–163.
- (42) Alimohamadi, H.; de Anda, J.; Lee, M. W.; Schmidt, N. W.; Mandal, T.; Wong, G. C. L. How Cell-Penetrating Peptides Behave Differently from Pore-Forming Peptides: Structure and Stability of Induced Transmembrane Pores. J. Am. Chem. Soc. 2023, 145, 26095.
- (43) Lipowsky, R. Budding of Membranes Induced by Intramembrane Domains. J. Phys. II France 1992, 2 (10), 1825–1840.
- (44) Saleem, M.; Morlot, S.; Hohendahl, A.; Manzi, J.; Lenz, M.; Roux, A. A Balance between Membrane Elasticity and Polymerization Energy Sets the Shape of Spherical Clathrin Coats. *Nat. Commun.* **2015**, *6* (1), 6249.
- (45) Frey, F.; Schwarz, S. U. Competing Pathways for the Invagination of Clathrin-Coated Membranes. *Soft Matter* **2020**, *16* (47), 10723–10733.
- (46) Ho, C. S.; Khadka, N. K.; She, F.; Cai, J.; Pan, J. Influenza M2 Transmembrane Domain Senses Membrane Heterogeneity and Enhances Membrane Curvature. *Langmuir* **2016**, 32 (26), 6730–6738.
- (47) Allain, J.-M.; Ben Amar, M. Budding and Fission of a Multiphase Vesicle. Eur. Phys. J. E Soft Matter 2006, 20 (4), 409–420.

- (48) Takei, K.; Mundigl, O.; Daniell, L.; De Camilli, P. The Synaptic Vesicle Cycle: A Single Vesicle Budding Step Involving Clathrin and Dynamin. *J. Cell Biol.* **1996**, *133* (6), 1237–1250.
- (49) Molina, R. R.; Liese, S.; Alimohamadi, H.; Rangamani, P.; Carlson, A. Diffuso-Kinetic Membrane Budding Dynamics. *Soft Matter* **2020**, *16* (48), 10889–10899.
- (50) Alimohamadi, H. Application of Continuum Mechanics for a Variety of Curvature Generation Phenomena in Cell Biophysics; University of California: San Diego, 2021.
- (51) Alimohamadi, H.; Rangamani, P. Effective Cell Membrane Tension Protects Red Blood Cells against Malaria Invasion. *PLOS Computational Biology* **2023**, *19* (12), No. e1011694.
- (52) Nakamura, Y.; Kulkarni, N. N.; Takahashi, T.; Alimohamadi, H.; Dokoshi, T.; Liu, E.; Shia, M.; Numata, T.; Luo, E. W.; Gombart, A. F.; Yang, X.; Secrest, P.; Gordts, P. L.; Tsimikas, S.; Wong, G. C.; Gallo, R. L. Increased LL37 in Psoriasis and Other Inflammatory Disorders Promotes LDL Uptake and Atherosclerosis. *J. Clin Invest* 2024, 134 (5), No. e172578.
- (53) Yuan, F.; Alimohamadi, H.; Bakka, B.; Trementozzi, A. N.; Day, K. J.; Fawzi, N. L.; Rangamani, P.; Stachowiak, J. C. Membrane Bending by Protein Phase Separation. *Proc. Natl. Acad. Sci. U.S.A.* **2021**, *118* (11), No. e2017435118.
- (54) Ferguson, S.; Raimondi, A.; Paradise, S.; Shen, H.; Mesaki, K.; Ferguson, A.; Destaing, O.; Ko, G.; Takasaki, J.; Cremona, O.; O'Toole, E.; De Camilli, P. Coordinated Actions of Actin and BAR Proteins Upstream of Dynamin at Endocytic Clathrin-Coated Pits. *Developmental Cell* **2009**, *17* (6), 811–822.
- (55) Kanso, M. A.; Naime, M.; Chaurasia, V.; Tontiwattanakul, K.; Fried, E.; Giacomin, A. J. Coronavirus Pleomorphism. *Phys. Fluids* **2022**, *34* (6), No. 063101.
- (56) Noda, T.; Ebihara, H.; Muramoto, Y.; Fujii, K.; Takada, A.; Sagara, H.; Kim, J. H.; Kida, H.; Feldmann, H.; Kawaoka, Y. Assembly and Budding of Ebolavirus. *PLOS Pathogens* **2006**, *2* (9), No. e99.
- (57) Welsch, S.; Kolesnikova, L.; Krähling, V.; Riches, J. D.; Becker, S.; Briggs, J. A. G. Electron Tomography Reveals the Steps in Filovirus Budding. *PLOS Pathogens* **2010**, *6* (4), No. e1000875.
- (58) Cureton, D. K.; Massol, R. H.; Saffarian, S.; Kirchhausen, T. L.; Whelan, S. P. J. Vesicular Stomatitis Virus Enters Cells through Vesicles Incompletely Coated with Clathrin That Depend upon Actin for Internalization. *PLOS Pathogens* **2009**, *5* (4), No. e1000394.
- (59) Ge, P.; Tsao, J.; Schein, S.; Green, T. J.; Luo, M.; Zhou, Z. H. Cryo-EM Model of the Bullet-Shaped Vesicular Stomatitis Virus. *Science* **2010**, 327 (5966), 689–693.
- (60) Badham, M. The Role of the Cytoplasmic Tail of the Influenza Virus M2 Protein in Viral Morphology and Replication. PhD, University of Kent, 2018. 10/1/75Matthew%20D%20Badham%20PhD%20Thesis.pdf.
- (61) Bahrami, A. H.; Raatz, M.; Agudo-Canalejo, J.; Michel, R.; Curtis, E. M.; Hall, C. K.; Gradzielski, M.; Lipowsky, R.; Weikl, T. R. Wrapping of Nanoparticles by Membranes. *Adv. Colloid Interface Sci.* **2014**, 208, 214–224.
- (62) Sadhu, R. K.; Barger, S. R.; Penič, S.; Iglič, A.; Krendel, M.; Gauthier, N. C.; Gov, N. S. A Theoretical Model of Efficient Phagocytosis Driven by Curved Membrane Proteins and Active Cytoskeleton Forces. *Soft Matter* **2022**, *19* (1), 31–43.
- (63) Champion, J. A.; Mitragotri, S. Role of Target Geometry in Phagocytosis. *Proc. Natl. Acad. Sci. U. S. A.* **2006**, *103* (13), 4930–4934.
- (64) Chan, E. Y. L.; McQuibban, G. A. Phosphatidylserine Decarboxylase 1 (Psd1) Promotes Mitochondrial Fusion by Regulating the Biophysical Properties of the Mitochondrial Membrane and Alternative Topogenesis of Mitochondrial Genome Maintenance Protein 1 (Mgm1). *J. Biol. Chem.* **2012**, 287 (48), 40131–40139.
- (65) Macdonald, P. J.; Stepanyants, N.; Mehrotra, N.; Mears, J. A.; Qi, X.; Sesaki, H.; Ramachandran, R. A Dimeric Equilibrium Intermediate Nucleates Drp1 Reassembly on Mitochondrial Membranes for Fission. *Mol. Biol. Cell* **2014**, 25 (12), 1905–1915.

- (66) Joshi, A. S.; Thompson, M. N.; Fei, N.; Hüttemann, M.; Greenberg, M. L. Cardiolipin and Mitochondrial Phosphatidylethanolamine Have Overlapping Functions in Mitochondrial Fusion in Saccharomyces Cerevisiae. *J. Biol. Chem.* **2012**, 287 (21), 17589–17597.
- (67) Mattila, J.-P.; Shnyrova, A. V.; Sundborger, A. C.; Hortelano, E. R.; Fuhrmans, M.; Neumann, S.; Müller, M.; Hinshaw, J. E.; Schmid, S. L.; Frolov, V. A. A Hemi-Fission Intermediate Links Two Mechanistically Distinct Stages of Membrane Fission. *Nature* **2015**, 524 (7563), 109–113.
- (68) Ramachandran, R.; Pucadyil, T. J.; Liu, Y.-W.; Acharya, S.; Leonard, M.; Lukiyanchuk, V.; Schmid, S. L. Membrane Insertion of the Pleckstrin Homology Domain Variable Loop 1 Is Critical for Dynamin-Catalyzed Vesicle Scission. *Mol. Biol. Cell* **2009**, 20 (22), 4630–4639.
- (69) Zhang, P.; Hinshaw, J. E. Three-Dimensional Reconstruction of Dynamin in the Constricted State. *Nat. Cell Biol.* **2001**, 3 (10), 922–926.
- (70) Chen, Y.-J.; Zhang, P.; Egelman, E. H.; Hinshaw, J. E. The Stalk Region of Dynamin Drives the Constriction of Dynamin Tubes. *Nat. Struct Mol. Biol.* **2004**, *11* (6), 574–575.
- (71) Nguyen, P. A.; Soto, C. S.; Polishchuk, A.; Caputo, G. A.; Tatko, C. D.; Ma, C.; Ohigashi, Y.; Pinto, L. H.; DeGrado, W. F.; Howard, K. P. pH-Induced Conformational Change of the Influenza M2 Protein C-Terminal Domain. *Biochemistry* **2008**, *47* (38), 9934–9936
- (72) Lee, E. Y.; Fulan, B. M.; Wong, G. C. L.; Ferguson, A. L. Mapping Membrane Activity in Undiscovered Peptide Sequence Space Using Machine Learning. *Proc. Natl. Acad. Sci. U. S. A.* **2016**, 113 (48), 13588–13593.
- (73) Gowers, R. J.; Linke, M.; Barnoud, J.; Reddy, T. J. E.; Melo, M. N.; Seyler, S. L.; Domanski, J.; Dotson, D. L.; Buchoux, S.; Kenney, I. M.; Beckstein, O. MDAnalysis: A Python Package for the Rapid Analysis of Molecular Dynamics Simulations; LA-UR-19—29136; Los Alamos National Lab. (LANL): Los Alamos, NM (United States), 2019.
- (74) Roux, A.; Uyhazi, K.; Frost, A.; De Camilli, P. GTP-Dependent Twisting of Dynamin Implicates Constriction and Tension in Membrane Fission. *Nature* **2006**, 441 (7092), 528–531.
- (75) Grassart, A.; Cheng, A. T.; Hong, S. H.; Zhang, F.; Zenzer, N.; Feng, Y.; Briner, D. M.; Davis, G. D.; Malkov, D.; Drubin, D. G. Actin and Dynamin2 Dynamics and Interplay during Clathrin-Mediated Endocytosis. *J. Cell Biol.* **2014**, 205 (5), 721–735.
- (76) Alimohamadi, H.; De Anda, J.; Lee, M. W.; Schmidt, N. W.; Mandal, T.; Wong, G. C. L. Deducing Size and Stability of Peptide-Induced Transmembrane Pores from Structure and Phase Behavior of Peptide-Lipid Systems. In *Bulletin of the American Physical Society*; Session G34: Emulsions, Micelles and Vesicles; American Physical Society: Minneapolis, MN, 2024.
- (77) Sandvig, K.; Olsnes, S. Diphtheria Toxin Entry into Cells Is Facilitated by Low pH. *J. Cell Biol.* **1980**, *87* (3 Pt 1), 828–832.
- (78) Zhu, C.; Lee, C. T.; Rangamani, P. Mem3DG: Modeling Membrane Mechanochemical Dynamics in 3D Using Discrete Differential Geometry. *Biophysical Reports* **2022**, *2* (3), No. 100062.
- (79) Mahapatra, A.; Saintillan, D.; Rangamani, P. Transport Phenomena in Fluid Films with Curvature Elasticity. *J. Fluid Mech.* **2020**, *905*, A8.
- (80) Iglič, A.; Hägerstrand, H.; Veranič, P.; Plemenitaš, A.; Kralj-Iglič, V. Curvature-Induced Accumulation of Anisotropic Membrane Components and Raft Formation in Cylindrical Membrane Protrusions. J. Theor. Biol. 2006, 240 (3), 368–373.
- (81) Agostinelli, D.; Elfring, G. J.; Bacca, M. The Morphological Role of Ligand Inhibitors in Blocking Receptor- and Clathrin-Mediated Endocytosis. *Soft Matter* **2022**, *18* (18), 3531–3545.
- (82) Lerner, D. M.; Deutsch, J. M.; Oster, G. F. How Does a Virus Bud? *Biophys. J.* **1993**, *65* (1), 73–79.
- (83) Tzlil, S.; Deserno, M.; Gelbart, W. M.; Ben-Shaul, A. A Statistical-Thermodynamic Model of Viral Budding. *Biophys. J.* **2004**, 86 (4), 2037–2048.

- (84) Bacca, M. Mechanics of Diffusion-Mediated Budding and Implications for Virus Replication and Infection. *Journal of The Royal Society Interface* **2022**, *19* (196), No. 20220525.
- (85) Helfrich, W. Elastic Properties of Lipid Bilayers: Theory and Possible Experiments. Z. Naturforsch C 1973, 28 (11), 693-703.
- (86) Deuling, H. J.; Helfrich, W. The Curvature Elasticity of Fluid Membranes: A Catalogue of Vesicle Shapes. *J. Phys.* (*Paris*) **1976**, 37 (11), 1335–1345.
- (87) Madsen, J. J.; Grime, J. M. A.; Rossman, J. S.; Voth, G. A. Entropic Forces Drive Clustering and Spatial Localization of Influenza A M2 during Viral Budding. *Proc. Natl. Acad. Sci. U. S. A.* **2018**, *115* (37), E8595—E8603.
- (88) Mears, J. A.; Lackner, L. L.; Fang, S.; Ingerman, E.; Nunnari, J.; Hinshaw, J. E. Conformational Changes in Dnm1 Support a Contractile Mechanism for Mitochondrial Fission. *Nat. Struct Mol. Biol.* **2011**, *18* (1), 20–26.
- (89) Alberts, B.; Johnson, A.; Lewis, J.; Raff, M.; Roberts, K.; Walter, P. *Mol. Biol. Cell*, 4th ed.; Garland Science, 2002.
- (90) Derjaguin, B. V. Theory of Stability of Colloids and Thin Films; Springer-Verlag: US: New York, NY, 1989.
- (91) Alimohamadi, H.; Smith, A. S.; Nowak, R. B.; Fowler, V. M.; Rangamani, P. Non-Uniform Distribution of Myosin-Mediated Forces Governs Red Blood Cell Membrane Curvature through Tension Modulation. *PLOS Computational Biology* **2020**, *16* (5), No. e1007890.
- (92) Alimohamadi, H.; Bell, M. K.; Halpain, S.; Rangamani, P. Mechanical Principles Governing the Shapes of Dendritic Spines. *Frontiers in Physiology* **2021**, *12*, No. 657074.
- (93) Iglič, A.; Slivnik, T.; Kralj-Iglič, V. Elastic Properties of Biological Membranes Influenced by Attached Proteins. *J. Biomech.* **2007**, *40* (11), 2492–2500.
- (94) Kralj-iglič, V.; Heinrich, V.; Svetina, S.; Žekš, B. Free Energy of Closed Membrane with Anisotropic Inclusions. *European Physical Journal B* **1999**, *10*, 5–8.
- (95) Baumgart, T.; Hess, S. T.; Webb, W. W. Imaging Coexisting Fluid Domains in Biomembrane Models Coupling Curvature and Line Tension. *Nature* **2003**, 425 (6960), 821–824.
- (96) Liu, J.; Kaksonen, M.; Drubin, D. G.; Oster, G. Endocytic Vesicle Scission by Lipid Phase Boundary Forces. *Proc. Natl. Acad. Sci. U. S. A.* **2006**, *103* (27), 10277–10282.
- (97) Walani, N.; Torres, J.; Agrawal, A. Anisotropic Spontaneous Curvatures in Lipid Membranes. *Phys. Rev. E Stat Nonlin Soft Matter Phys.* **2014**, 89 (6), No. 062715.
- (98) Bobrovska, N.; Góźdź, W.; Kralj-Iglič, V.; Iglič, A. On the Role of Anisotropy of Membrane Components in Formation and Stabilization of Tubular Structures in Multicomponent Membranes. *PLoS One* **2013**, *8* (9), No. e73941.
- (99) Iglič, A.; Babnik, B.; Gimsa, U.; Kralj-Iglič, V. On the Role of Membrane Anisotropy in the Beading Transition of Undulated Tubular Membrane Structures. *J. Phys. A: Math. Gen.* **2005**, 38 (40), 8527–8536.
- (100) Rawicz, W.; Olbrich, K. C.; McIntosh, T.; Needham, D.; Evans, E. Effect of Chain Length and Unsaturation on Elasticity of Lipid Bilayers. *Biophys. J.* **2000**, *79* (1), 328–339.
- (101) Hu, M.; Briguglio, J. J.; Deserno, M. Determining the Gaussian Curvature Modulus of Lipid Membranes in Simulations. *Biophys. J.* **2012**, *102* (6), 1403–1410.
- (102) Harper, P. E.; Gruner, S. M. Electron Density Modeling and Reconstruction of Infinite Periodic Minimal Surfaces (IPMS) Based Phases in Lipid-Water Systems. I. Modeling IPMS-Based Phases. *Eur. Phys. J. E* **2000**, 2 (3), 217–228.
- (103) Schwarz, U. S.; Gompper, G. Systematic Approach to Bicontinuous Cubic Phases in Ternary Amphiphilic Systems. *Phys. Rev. E* **1999**, *59* (5), 5528–5541.